The role of land-surface processes in modulating the Indian monsoon annual cycle

The role of land-surface processes in modulating the Indian monsoon annual cycle

Massimo A. Bollasina[1,*] and Yi Ming[2]

[1]*Program in Atmospheric and Oceanic Sciences, Princeton University,*

300 Forrestal Road, Sayre Hall, Princeton, NJ 08540

[2]*Geophysical Fluid Dynamics Laboratory/NOAA*

201 Forrestal Road, Princeton, NJ 08540

Submitted to *Climate Dynamics* on July 18, 2012; revised on October 22, 2012

*Corresponding author:

E-mail: massimo.bollasina@noaa.gov

Keywords: Indian monsoon annual cycle; land-atmosphere interactions; perpetual experiments

ABSTRACT

The annual cycle of solar radiation, together with the resulting land-ocean differential heating, is traditionally considered the dominant forcing controlling the northward progression of the Indian monsoon. This study makes use of a state-of-the-art atmospheric general circulation model in a realistic configuration to conduct "perpetual" experiments aimed at providing new insights into the role of land-atmosphere processes in modulating the annual cycle of precipitation over India. The simulations are carried out at three important stages of the monsoon cycle: March, May, and July. Insolation and SSTs are held fixed at their respective monthly mean values, thus eliminating any external seasonal forcing.

In the perpetual May experiment both precipitation and circulation are able to considerably evolve only by regional internal land-atmosphere processes and the mediation of soil hydrology. A large-scale equilibrium state is reached after approximately 270 days, closely resembling mid-summer climatological conditions. As a result, despite the absence of external forcing, intense and widespread rains over India are able to develop in the May-like state. The interaction between soil moisture and circulation, modulated by surface heating over the northwestern semi-arid areas, determines a slow northwestward migration of the monsoon, a crucial feature for the existence of desert regions to the west. This also implies that the land-atmosphere system in May is far from being in equilibrium with the external forcing. The inland migration of the precipitation front comprises a succession of large-scale 35-50 day coupled oscillations between soil moisture, precipitation, and circulation. The oscillatory regime is self-sustained and entirely due to the internal dynamics of the system.

In contrast to the May case, minor changes in the land-atmosphere system are found when the model is initialized in March and, more surprisingly, in July, the latter case further emphasizing the role of northwestern surface heating.

1. Introduction

The Asian summer monsoon (ASM) is a manifestation of the strong annual cycle that exists over the region, which results in a remarkable meridional shift of the intertropical convergence zone (ITCZ; e.g., Goswami et al. 2006). Monsoon precipitation is of vital importance for more than 60% of the world's population and the mainly agrarian society which strongly relies on it. The Indian summer monsoon (ISM), one of the two major regional subsystems of the ASM (the other being the East Asian monsoon), is the focus of this study. The two systems are largely independent of each other, and differ in land-ocean distribution, topographic forcing, and interaction with the mid-latitudes (e.g., Wang et al. 2003).

The ISM is a fully-coupled ocean-atmosphere-land phenomenon whose complexity is manifested for example in its seasonal cycle which, despite the smooth evolution in solar forcing, includes an abrupt onset of monsoon precipitation (e.g., Ueda 2005) as well as changes in the large-scale atmospheric circulation. The onset in early summer is of paramount importance since it heralds the beginning of the rainy season over the dry Indian sub-continent. Figure 1, based on pentad observational data, depicts some salient features of the ISM annual cycle. Precipitation is zonally-averaged across the Indian peninsula, sea surface temperature (SST) over the western Indian Ocean (IO), and the wind over the core region of the Arabian Sea low-level jet (e.g., Goswami 2005; Ueda 2005). In early May, low-level northwesterlies blow over India, reminiscent of the winter regime, and precipitation is mainly located along the equatorial IO. Warm SSTs extend across the north equatorial IO lagging the march of solar radiation. The "first transition" of the monsoon occurs just after mid-May, and consists of a northward shift and enhancement of convection, and a simultaneous acceleration of the westerly wind in the band 0°-10°N (the area of warmest SSTs prior to the transition). A series of

sudden changes in precipitation and low-level circulation take places in the following month and lead to the establishment of the ISM over central India by the middle of June (e.g., Goswami 2005). Overall, substantial precipitation has migrated northward to about 25°N, with an increase over central India by about 5 mm day^{-1}. Correspondingly, strong low-level westerlies blow in the 10°-20°N band across the basin. Note that once the monsoon circulation commences, enhanced coastal upwelling and evaporation associated with the strengthened westerly monsoon flow lead to SST cooling.

The most fundamental and simplistic paradigm views the monsoon as a planetary-scale land-sea breeze circulation driven by the land-ocean thermal contrast developing in response to the annual cycle of solar forcing and due to their different thermal properties (e.g., Webster et al. 1998). However, the gradual variation of solar radiation does not explain by itself, for example, either the abruptness of the onset or its delay with respect to the evolution of the land-ocean contrast, or why the rain zone does not extend as far poleward as the maximum insolation would indicate.

Regional SSTs modulate the land-ocean thermal difference and, additionally, influence the monsoon by affecting surface heat and moisture fluxes, and by inducing, through air-sea interactions, anomalous elevated atmospheric heat sources and associated Rossby wave propagation (e.g., Yang and Lau 2006). For example, warm SST over the Arabian Sea has been shown to favor the monsoon onset (e.g., Ueda 2005). The northward seasonal march of the warm SST tongue has also been suggested to lead the movement of the monsoon rainfall (e.g., Wu and Wang 2001; see also Fig. 1). Observations and simplified modeling experiments, however, have suggested that the role of the annual cycle of SSTs in the establishment of the monsoon circulation, albeit important, is in general secondary to that due to the response of the land-atmosphere system to insolation (e.g., Shukla and Fennessy 1994; Sud et al. 2002; Ueda 2005; Lestari and Iwasaki 2006; Ueda et al. 2009; Jiang and Li 2011).

Internal nonlinear processes of the land-atmosphere system (i.e., surface processes, atmospheric transients) have been advocated as important for the monsoon cycle (e.g., Wu and Wang 2001; Ueda et

al. 2009). Land-surface anomalies (i.e., snow cover, soil moisture, vegetation cover) affect the monsoon by altering the surface water and energy budgets, which influence the availability of water over the land (typically dry before the monsoon onset), its heating and stability (e.g., Yang and Lau 2006). These issues have been extensively investigated in observational and modeling studies in various contexts (i.e., from the intraseasonal to the interdedacal scale). Yet, the multifaceted roles of land-surface processes in the South Asian monsoon system are not yet well understood (see for example Yasunari (2007) for a review).

This study aims at providing new insights into one of these roles, namely how regional land-surface processes modulate the inland northward progression of the ISM rainfall. The onset phase is particularly targeted, given its importance as transition from dry to wet conditions. Considering solar radiation and SSTs as *external* forcings on the annual cycle of precipitation over the land (locally, in case of the sun; remotely via large-scale circulations, in case of the SSTs), we want to address the following question: to what extent do *internal* land-atmosphere interactions contribute to establishing the monsoon regime? In other words, to what extent is the monsoon able to progress by the effect of land-atmosphere processes only, while solar radiation and SSTs are not allowed to vary through their annual cycle?

An interesting and related issue is how land-atmosphere processes are brought into play in the presence of the external forcing (e.g., Xie and Saiki 1999; Mapes et al. 2005). The land-atmosphere system might be in local equilibrium with solar insolation and SSTs but have a strong response at specific times of the year (function of the external large-scale conditions) and thus leading to a substantial and rapid change in the monsoon (such as at the time of the ISM onset). Alternatively, the absence of equilibrium would imply that land-atmosphere interactions have internal sub-seasonal variations which make it possible for them to evolve independently, once initiated.

This study makes use of a set of perpetual experiments with a state-of-the-art atmospheric general

circulation model (AGCM) to investigate the above issues. Perpetual experiments with fixed insolation and SST allow studying the contribution of individual forcings to the overall annual cycle (e.g., Xie and Saiki 1999; Biasutti et al. 2003). Three representative moments are examined: March (the transition between winter and pre-monsoon conditions), May (just before the monsoon onset over India), and July (when the monsoon is in full swing).

This work builds upon the findings of earlier studies which previously documented the existence of disequilibrium in the land-atmosphere system with respect to the external forcing and the role of slow hydrological processes in dictating the northward migration of the monsoon rainbelt (e.g., Zwiers and Boer 1997; Xie and Saiki 1999; Mapes et al. 2005). Yet, our experiments are carried out with a state-of-the-art AGCM and in a realistic configuration, which substantially improves previous idealized or rather simplified settings (Zwiers and Boer 1997; Xie and Saiki 1999), including the parameterization of hydrological processes. These features are important for highlighting the role and details of key regional processes at play (e.g., the pattern of surface heating, the contribution of moisture recycling and evaporation, the orographic forcing), and provide more confidence in interpreting the results and their applicability to the actual monsoon. We argue that these aspects are responsible for the interesting finding that the largest disequilibrium occurs in May rather than in July as in Xie and Saiki (1999). We also more comprehensively describe the mechanism through which the land-atmosphere system adjusts toward equilibrium (for example only briefly discussed in Mapes et al. 2005) and its realization, at subseasonal time-scales, through a land-atmosphere coupled oscillation (previously discussed in very simplified and ideal studies; e.g., Abbott and Emanuel 2007). Overall, this study provides new insights into the fundamental physics of the monsoon annual cycle and the role of *regional* land-atmosphere processes in the framework of the large-scale monsoon system.

The article is organized as follows: Section 2 provides a detailed description of the model used and the simulations strategy. Section 3 describes the experimental results, most notably the transient nature

of the land-atmosphere system at the onset stage of the simulated monsoon. The role played by land-atmosphere processes in determining the progressive drift in the simulated monsoon is highlighted, and a discussion follows in Section 4. Summary and concluding remarks follow in Section 5.

2. Model, Experiments, and Observational Datasets

The AGCM used in this study is the latest Geophysical Fluid Dynamics Laboratory (GFDL) atmospheric model AM3, the atmospheric component of the GFDL climate model (CM3). Some key features of AM3 compared to the previous GFDL models are: a new treatment of deep and shallow cumulus convection, an improved land model, a parameterization of cloud-droplet activation by aerosols, a parameterization of sub-grid variability of vertical velocities, and fully interactive cloud-aerosols effects and chemistry. The horizontal resolution is 2° x 2.5°, with 48 vertical levels. A detailed description of the model, its physical parameterizations, as well as a preliminary evaluation of its overall performance can be found in Donner et al. (2011).

The control run (CTL) consists of a 7-yr simulation with monthly-varying climatological (1981-2000) observed SST derived from the HadISST1 observational dataset (Rayner et al. 2003), with the first year disregarded as model spin-up. The salient features of the CTL simulated climatological South Asian summer monsoon are compared to long-term (1981-2000 average) observations of precipitation (the Climate Prediction Center (CPC) Merged Analysis of Precipitation (CMAP; Xie and Arkin 1997) observation-only product) and atmospheric circulation (the European Centre for Medium-Range Weather Forecasts (ECMWF) Reanalysis (ERA-40; Uppala et al. 2005) to evaluate its suitability for monsoon studies. The CTL run also provides a reference against which the experiments described below can be directly compared.

The response of the ISM to land-atmosphere processes is studied by means of AM3 simulations in perpetual (PER) mode, with insolation and SSTs held fixed at their monthly mean values (e.g., Zwiers and Boer 1987; Hagos and Cook 2005). Three perpetual simulations, initialized on 1 March, 1 May, and 1 July, are run for several hundred days each. Correspondingly, daily insolation and SSTs are kept fixed at their March, May, and July mean values, respectively. Each simulation is initialized from the CTL run, so there is no need for spin-up. The results are presented in the form of averages over 5 (pentad) or 30-day (monthly) consecutive intervals. For each experiment, the statistical significance of the changes with respect to the initial condition is assessed by means of the Student's *t*-test for the difference of the means with equal variances.

3. Monsoon onset and unsteady response

3.1 The control run

In view of the modeling perspective adopted in this study, an important first step is to evaluate the AM3's skill in simulating the basic features of the ISM. The CTL simulated annual march of precipitation over the Indian sector (Fig. 2b) is compared with the observational counterpart (Fig. 2a). The migration of the rain belt from its wintertime location south of the equator to its summertime position at ~15°N and the timing of the monsoon onset are realistically simulated, with little interannual variability in the timing (see the black lines in Fig. 2b). The model tends to produce excessive orographic precipitation along the Himalayas, and to overestimate the mid-summer amount over central India[1]. The monsoon withdrawal is also more gradual than observed. Panels (c) and (d) of

[1] Further analysis (not shown) indicates that these biases are altogether comparable to those of other state-of-the-art AGCMs from the Coupled Models Intercomparison Project (CMIP) 3 archive, as well as to the spread of the observational estimates.

Fig. 2 show the comparison between the observed and simulated spatial patterns of precipitation and 850-hPa winds for May, which sets the stage for the monsoon onset. The major features, such as the position of the 5mm day^{-1} rain contour across southern India and the Bay of Bengal, and the precipitation band at about 5°N, are well-captured by the model. We note that the dry bias over the southern Bay of Bengal and the eastern equatorial India Ocean is partly related to uncertainties in the observational estimates.[2] Both magnitude and direction of the simulated flow depict the observed warm moist north-equatorial westerlies turning to southwesterlies in the Bay of Bengal, and the dry northwesterlies over India. The simulated transition to the monsoon regime is shown in Fig. 2e. A strong southwesterly wind flows over the Arabian Sea, across India and the southern Bay of Bengal. The wind turns cyclonically in the northern Bay of Bengal, bringing moisture to northern India. In good agreement with observations (not shown), precipitation decreases along the equator and substantially increases north of 10°N, especially off the western coast of India and the northern Bay of Bengal/northeastern India. The May to June precipitation increase over the core monsoon region (75°-85°E, 20°-25°N) is 6.0 mm day^{-1} in CTL, reasonably close to the observational estimates (4.1, 4.7, 4.8 mm day^{-1} using CMAP, GPCP, and TRMM 3B43, respectively). The use of climatological instead of monthly-varying SST has certainly its impact, since the same AGCM run with observed monthly interannual-varying SST gives 4.8 mm day^{-1}.

The above analysis, albeit by no means exhaustive, shows that the model is able to reproduce the major features of precipitation and circulation over the region with biases comparable to other AGCMs (e.g., Kang et al. 2002; Meehl et al. 2006).

[2] Other two observational datasets, namely the Global Precipitation Climatology Project (GPCP) version 2 and the Tropical Rainfall Measuring Mission (TRMM) 3B43, show lower precipitation amounts over the Bay of Bengal and the eastern equatorial Indian Ocean (e.g., Xie et al. 2006).

3.2 The perpetual runs

In this section we analyze the development of the monsoon as simulated by perpetual runs. We also investigate the existence of equilibrium in the land-atmosphere system, and how the model evolves toward it. The role of land-surface processes in driving the adjustment is discussed.

3.2.1 Unsteadiness of the monsoon development

Both the transient response and the equilibrium solution are analyzed, as they both provide important insights into the impact of land-atmosphere processes on the monsoon. Considering the May run, the difference between the first two 30-day increments should be directly compared to the May-to-June transition of the actual monsoon system. On the other hand, the equilibrium solution should be interpreted as steady-state solution to a time-independent (climatological) boundary value problem. As there is no annual cycle forcing in the perpetual integrations, if the land-atmosphere system is initially in equilibrium, no *substantial* change should be observed in the perpetual run. In other words, the perpetual run would essentially reproduce the mean circulation for that specific month simulated by CTL (e.g., Zwiers and Boer 1987). However, this might not necessarily occur, and the difference with respect to the initial state should be interpreted as the effect of internal feedbacks of the land-atmosphere system operating at sub-seasonal time scale.

Figure 2f shows that the large-scale patterns of precipitation and circulation averaged over the first month of the May perpetual experiment are very similar to the CTL ones (Fig. 2d), especially over the continent. Due to the tendency of Indian Ocean SSTs (especially around 10°N) to progressively cool from mid-May, the perpetual experiment (Fig. 2f) tends to produce slightly more oceanic precipitation than CTL (Fig. 2d) due to warmer SSTs forcing.

Figure 3 presents the evolution of precipitation and 850-hPa winds in the perpetual experiments. The left column shows the time-latitude variations of these two variables for (from top to bottom) May, March, and July. As for Fig. 1, precipitation is zonally averaged over the Indian subcontinent, while wind is averaged over the area of the core of the summertime low-level jet over the Arabian Sea.

The most remarkable feature is noticeable in the May experiment (Fig. 3a): both precipitation and winds rapidly migrate northward, and then locally intensify, with maximum values occurring after about 210 days of simulation (t = 7). Afterwards, both variables reduce slightly in magnitude and then undergo local (i.e., without an appreciable meridional shift) small amplitude oscillations. In other words, the system behaves like a damped oscillator. Ignoring for the moment these fluctuations (whose magnitude is clearly of second order compared to the overall change from the initial state; see Section 3.2.3 for a thorough analysis of the oscillatory regime), the system can be thought of reaching a *large-scale* equilibrium state after about 270 days[3]. At equilibrium (defined as the average between 270-330 days (t = 9-11)), precipitation and winds are substantially different from the initial condition; for example, the 8 mm day^{-1} precipitation contour, initially located at ~12°N, has moved northward to ~28°N, and the average amount in the 15°-25°N band (central India) has more than doubled (from 4.3 to 8.9 mm day^{-1}). Correspondingly, the band of lower-tropospheric westerlies, initially located between the equator and 10°N, has progressively extended to the north and turned to southwesterlies and intensified (the magnitude of the wind almost doubled between 5°-15°N). The spatial patterns of the changes are shown in Figs. 3b (the first adjustment) and 3c (equilibrium) as differences with respect to the initial condition (Fig. 2f). Already after about 30 days, the simulated precipitation and winds show a clear tendency to evolve toward June-like conditions (compare Fig. 3b to Fig. 2e), with a substantial increase of precipitation off the west coast of India and over the central regions (+4.8 mm day^{-1} over

[3] The amplitude of the oscillations at about 300 days is modest on a large-scale average compared to the overall drift from the initial condition (the transient response), and it is thus reasonable to consider these states as approximately in equilibrium.

the area 75°-85°E, 20°-25°N), accompanied by an intensified moist flow across the Arabian Sea and southern India. At equilibrium, precipitation has further increased (additional 2.4 mm day^{-1} over the same area, for a total change of +7.3 mm day^{-1} from the initial state) and advanced north-northwestward.[4] Interestingly, the pattern of the changes is consistent throughout the simulation, with major increases occurring over the Arabian Sea and central-northern India. Correspondingly, the monsoon circulation over the region has intensified, and is associated with the deepening of the monsoon low over the northwestern arid regions (-6 hPa, not shown) and increased moisture advection from the Bay of Bengal. This suggests a relationship between the monsoon march and the heating over the western arid regions (e.g., Bollasina and Nigam 2011a), which will be further investigated in the next section. Note that SSTs do not change during the simulation, and the oceanic precipitation increase is linked to the stronger landward flow.

To better understand the mechanism driving the remarkable shift in the May experiment and to depict a more comprehensive physical picture of the monsoon annual cycle, two additional perpetual experiments were carried out for March and July. The respective evolution of precipitation and winds is also displayed in Figure 3. During March, the region is climatologically under the influence of a low-level anticyclonic flow featuring dry northwesterlies over India turning to northeasterlies to the south. Precipitation is confined to a zonal band south of 10°N, while the continent is very dry. As the perpetual simulation evolves (Figs. 3d-f), the model tends to progressively shift the oceanic precipitation band northeastward in response to the warming of the land and the appearance of a large-scale anomalous cyclonic flow over India. This indicates that the system tends to advance in the annual cycle also for March initial conditions, though the changes are not as large as during May. During July, the climatological monsoon is in its mature phase: strong moist southwesterlies blow across the Arabian Sea, turning cyclonically over the northern Bay of Bengal. In the corresponding perpetual

[4] For comparison, the May to Jun precipitation increase over the same region simulated by CTL is +7.1 mm day^{-1}.

experiment (Figs. 3g-i), before reaching equilibrium, precipitation undergoes two large-scale oscillations associated with substantial changes in circulation and related moisture advection. At first the climatological flow reinforces, resulting in a gradual northwestward expansion of the precipitation front until a maximum over northern India after about 90 days (t = 3). At this point the flow weakens, an anomalous anticyclone forms over northern India and precipitation decreases. The cycle then repeats until precipitation reaches a secondary maximum at t =7 (as for the May experiment) associated with a new gradual strengthening of the southeasterly cyclonic circulation over northern India. Note that the precipitation core does not extend as northward as for the first major peak (e.g., Fig. 3g). As the simulation evolves, an anomalous cyclonic circulation over southern India associated with local increased precipitation opposes the climatological moist flow, leading to an overall slight decrease of the core monsoon precipitation (Fig. 3i). Overall, as for the March experiment, the magnitude of the changes over the Indian subcontinent is relatively modest and the pattern is characterized by finer-scale features, contrasting the rather dramatic large-scale organized changes found in May.

In summary, these perpetual results show that significant shifts in rainfall and low-level circulation occur when the model is initialized in May. Despite a constant amount of solar radiation at the top of the atmosphere (i.e., the input of energy to the climate system), the circulation evolves toward the mature stage of the monsoon regime, which would otherwise occur about a month later in the climatology. During March the system evolves, but precipitation is not able to advance northward in a substantial way. To correctly interpret the outcomes of the March experiment, it is important to recall that insolation over the northern continent is much lower (< -60W m^{-2}) and SST over the northern Indian Ocean is much colder (< -2°C) than during May. These two factors play a fundamental role for the springtime northward migration of the equatorial precipitation band (e.g., Ueda 1995; Lestari and Iwasaki 2006), and their strong forcing represents a necessary condition for convection to be able to move over land. Conversely, though insolation is higher in July than in May (with SST deemed to play

a minor role once the monsoon has shifted northward over the land; e.g., Ueda et al. 2009), the additional amount of energy constantly added to the system is not able to ultimately significantly shift the monsoon northwestward (precipitation over central-northern India actually decreases; see Fig. 3i), regardless of the potentially favorable atmospheric conditions and the availability of moisture.

Land-surface processes and the coupling with the atmosphere through sensible and latent heat fluxes play an important role in initiating the northward precipitation migration and its subsequent intensification during May, a mechanism which we will explore in more detail in the next section. The same mechanism acts also in July initially to modulate and subsequently to limit the northwestward expansion of the precipitation front.

Note that the impact of land-surface processes is not confined to the land. Interestingly, and more clearly for May, land precipitation anomalies drive circulation anomalies that extend over the ocean and significantly affect intensity and location of the maritime precipitation band. Interestingly, these oceanic changes are broadly consistent with the climatological monsoon transition, suggesting an important remote forcing by the land in the actual system.

3.2.2 Land-atmosphere interactions and monsoon migration

Figure 4 shows the time-longitude variations of monthly mean variables meridionally averaged over central-northern India latitudes (20°-28°N), the area of large precipitation increase in the May simulation (see Fig. 3c), and provides insights into the mechanism driving the progressive shift of the precipitation front. Generally speaking, the initial condition features an eastward monotonic increase across the whole sector for the variables associated with humidity (e.g., precipitation, soil moisture, specific humidity), and a decrease for those associated with temperature (e.g., surface skin temperature, sensible heat flux), as the western regions are very dry.

The monsoon rain progressively advances westward until the maximum at 210 days (t = 7), then it undergoes a small amplitude oscillation accompanied by a modest eastward retreat before achieving equilibrium (Fig. 4a). Soil moisture increase accompanies the advancement of precipitation, with the eastern part of the domain becoming increasingly wetter. Note that a relatively wet ground (soil moisture fraction between 0.15-0.2) exists westward of the precipitation front (i.e., in the 70°-80°E longitudinal band) at the beginning. This appears to be fundamental for precipitation to be able to start propagating. Further support comes by considering the atmospheric water balance equation and the approximate balance (i.e., neglecting the storage term) between precipitation minus evaporation and column moisture flux convergence. Until about 120 days (t = 4) only evaporation (which depends on soil moisture) contributes to precipitation formation, while moisture fluxes diverge (Fig. 4b). A strong easterly moist wind starts supplying humidity (Figs. 4b and 4c) over northern India after about 150 days (t = 5); large moisture flux convergence is associated with the migration of the core monsoonal precipitation, and provides the major contribution to precipitation at the time of its peak. Interestingly, evaporation tends to peak after precipitation reaches its maximum value (when moisture transport and convergence also decrease). Furthermore, in the equilibrium phase, the evaporation maximum tends to be located westward of the maximum in precipitation, which in turn is westward of the front in moisture flux convergence.

Surface temperature (Fig. 4c) is maximum over the dry areas west of the migrating rainbelt and, as a result of the persistently strong solar radiation, increases until the peak at about 180 days (t =6), ahead of precipitation and moisture flux convergence. A similar variation is also found in the sensible heat flux (Fig. 4d). Interestingly, the area of maximum temperature is almost stationary in space and anchored to about 62°-70°E, which corresponds to the semi-arid region between Pakistan and northwestern India (enclosing the Thar Desert). For this reason, temperature starts decreasing when the precipitation front reaches the region. To the east of the precipitation front, evaporation and shielding of

solar radiation by clouds lead to a gradual cooling of the ground, resulting in a westward longitudinal gradient in temperature of more than 15°C across the domain. Temperature is the major contributor to moist static energy and, as a result, the latter has maximum values to the west of the precipitation front (Fig. 4d), which cause precipitation to advance (e.g., Xie and Saiki 1999).

Since surface heating of the semi-arid region between Pakistan and India is a key driving component of this mechanism, precipitation cannot expand indefinitely to the west. In other words, the migration is geographically confined: the realistic geographical setting of these experiments shows in fact that once precipitation starts cooling this key region, the front partially recedes to the east.

The same mechanism also modulates the precipitation progression in the July experiment (not shown). However, in this case, while the northwestern semi-arid regions rapidly warm-up in response to the strong insolation, it does not take long for precipitation to expand to the west, as its front is initially already advanced (e.g., the 2 mm day^{-1} contour is located at about 70°E over northern India at t = 1) and the flow is favorable. As a result, the land starts cooling at t = 3, followed by a slow down of the southeasterly moisture flux and by a decrease in precipitation. Temperature increases again initiating a second weaker cycle, as wetter conditions prevent the land to heat-up as before. The arrival of the second pulse of precipitation at t= 7 cools the land even further, determining a subsequent overall precipitation decrease compared to the initial condition. Moisture flux and its convergence plays the major role in modulating precipitation during July, while evaporation, being the soil wet most of the time, is relatively constant throughout the simulation.

3.2.3 An oscillation mechanism

A high-resolution temporal analysis allows for a better understanding of how the adjustment of the land-atmosphere system toward equilibrium is realized. Figure 5 displays the time series of important

variables at pentad resolution for the May experiment. The domain of averaging (except for the wind) is located over central-northern India (72°-85°E, 20°-25°N) and corresponds to the area of maximum precipitation increase in Figs. 3 and 4. As the increase in precipitation is associated with the formation of a cyclonic circulation over northeastern India and associated southerly moisture transport, the wind is shown in terms of its meridional component averaged over (85°-90°E, 15°-20°N).

Every variable displayed in Fig. 5 clearly shows variations at two major time scales, with a high-frequency quasi-periodic oscillatory regime superposed to a long-term growth (decay). The latter corresponds to the westward migration of precipitation described above, with the progressive relaxation toward equilibrium. The former is characterized by approximately regular oscillations with a period varying between 35-50 days (7-10 pentads). Note that the constant out-of-phase relationship among the variables is indicative of a possible driving mechanism which, in its essence, resembles the one described for example by Abbott and Emanuel (2007). Longer and larger-amplitude oscillations occur in the transient phase and, particularly, at the beginning, when the soil is drier and surface temperature is higher. After the region gets wetter by the migrating rainfall front, it is not able to heat up as in the early stages, and the oscillation becomes smaller and shorter. A lengthening of the oscillation period by increasing the soil field capacity (which is equivalent to decreasing its saturation) was found by Abbot and Emanuel (2007).

The spatial evolution of the oscillation over a 40-day period is represented in Figure 6, where each panel is 5 days apart. A 25-60 day bandpass filter was applied to the time series before computing the regressions in order to highlight variations at intraseasonal time scale. Beginning 20 days ahead of the precipitation maximum over central-northern India, a positive precipitation anomaly develops over the southern Bay of Bengal off the eastern coast of India (where initial large precipitation is located; see Fig. 2f), gradually moves northwestward toward the continent and intensifies, progressively replacing the negative precipitation anomaly. This migration is associated with a reversal of the circulation and

gradual intensification of a large-scale anomalous cyclonic flow over the continent, as well as the development of a positive temperature anomaly northwestward. Notice the core of positive temperature anomaly over Pakistan and its maximum value at lag -5 days; the southeasterly moist wind over northern India also peaks at that time. Notice also that the precipitation and wind patterns at t = 0 resemble those depicted in Fig. 3c, suggesting a link between the intraseasonal oscillation and the overall monsoon evolution. As the precipitation front reaches its westward maximum extension at t = 0, temperature starts decreasing, followed by the reduction of the easterly flow and, ultimately, the decrease of the precipitation anomaly. The wind then gradually reverses, opposing the climatological flow and leading to the largest negative precipitation anomaly at lag = +15 days. At this point, the cycle repeats. Interestingly, as the positive precipitation anomaly develops over the land, the anomaly over its genesis region in the southern Bay of Bengal reverses too. The oceanic oscillation, of smaller amplitude (about half) than the one over the land, is approximately in opposite phase (a phase difference of ~20 days) with the latter, and the two are linked by the oscillation in horizontal velocity and related landward moisture transport at the land-ocean interface (e.g., Srinivasan et al. 1993; Abbot and Emanuel 2007). Low-level moisture advection from the Bay of Bengal plays a crucial role for intense precipitation to develop since the contribution of local evaporation is about 40% after the initial stage (see also Fig. 4).

4. Discussion

The findings described above indicate that *regional* land-surface processes are a major player in regulating the initial progression of the monsoon over India. Similarly, Ueda et al. (2009) and Futami et al. (2009) found land memory effects over India to dominate solar radiation and SSTs effects during the

May-to-June transition of the Indian monsoon, determining almost entirely the continental precipitation change of the period. The regional climate modeling study of Saha et al. (2011) also concluded that soil moisture and associated land-surface processes can substantially modulate the first transition of the monsoon in early June.

We acknowledge that the global nature of the experiments described here does not allow us to isolate the contribution of regional and remote land-atmospheric processes to the changes over the Indian subcontinent. Although the two forcings are not directly separated (e.g., by performing simulations with land-atmosphere interactions enabled only over a specific region), we argue that the former plays a substantially larger role than the latter in driving the monsoon development in the May perpetual run. This is suggested by the pattern of the changes in sea level pressure and surface temperature, key elements of the monsoon circulation (e.g., Kripalani et al. 2007). As the simulation evolves, the northwestward migration of monsoon rainfall is associated with a very pronounced heating over northwestern India and the adjacent semi-arid areas, and the simultaneous progressive deepening of the regional low pressure system (not shown). The latter contributes to reinforcing the climatological cyclonic flow over the Arabian Sea and the Indian subcontinent. Conversely, the changes appear of much smaller amplitude elsewhere over the continent.

A cautionary remark is however necessary. The fact that the monsoon is able to progress in late spring despite SSTs being fixed to pre-onset conditions does not rule out the important contribution of (previous) oceanic conditions to the overall monsoon cycle. Springtime SST warming in the Arabian Sea sets up the necessary condition for the ITCZ jump from the southern to the northern hemisphere (e.g., Ueda 1995; Lestari and Iwasaki 2006) which precedes the monsoon onset (see also Section 3.2.1 and the March experiment). The May-June SST change has actually been suggested to exert a negative feedback on the monsoon convection (Ueda et al. 2009). In summer, when the monsoon is fully established, SST plays an important role for intraseasonal monsoon variations (e.g., Jiang and Li 2011;

Lau and Nath 2012).

The unsteadiness of the monsoon climate with respect to the seasonal evolving forcing and the 1-month delayed response agree with previous findings (e.g., Xie and Saiki 1999; Mapes et al. 2005). In their perpetual experiments, Xie and Saiki (1999) also emphasized the important role of soil hydrology in modulating the northward migration of the monsoon, but using a simplified GCM and a highly-idealized configuration. Interestingly, they find the largest disequilibrium in July while our experiments suggest it to occur in May as a result of the interaction between localized surface heating and precipitation progression. In their slowed-calendar experiments, Mapes et al. (2005), while not providing mechanistic details, highlighted the role of Eurasian continental temperature in driving the out-of-equilibrium response of the monsoon. Conversely, we show here that the monsoon migration is mostly driven by regional processes.

Earlier, Zwiers and Boer (1987) had also hypothesized ground water to be responsible for the large difference in their July perpetual simulation compared to an annually-forced case. The increase in monsoon precipitation over northern India in their 210-day July perpetual experiment is also present in our run at the corresponding time (not shown; see Fig. 3g at t = 7 for a zonal average)[5].

The mechanism for the monsoon oscillation had been previously discussed in the context of the intraseasonal variability of the monsoon maximum in convective activity (e.g., Webster 1983; Srinivasan et al. 1993), albeit in a very simplified and ideal setting. A soil moisture oscillation mechanism in the tropical and subtropical land-sea regions was also suggested by the idealized modeling study of Abbott and Emanuel (2007). Conversely, Ferranti et al. (1999), using July perpetual simulations, did not find surface hydrological processes to be important for the existence of

[5] As our simulation progresses, it tends to reduce precipitation over India, leading to the slightly negative change shown in Fig. 3i. This apparent discrepancy with Zwiers and Boer (1987) could be related to a number of factors which affect the different time-scale of the adjustment toward equilibrium in the two models, including the rather simplified parameterization of hydrological processes (a bucket model) in Zwiers and Boer (1987).

intraseasonal northward-propagating monsoon convective events, though hydrology affected frequency and amplitude of these events.

5. Summary and conclusions

This study describes a set of perpetual AGCM experiments aimed at providing new insights into the role of regional land-atmosphere processes in modulating the annual cycle of monsoon precipitation over India, especially the considerable inland march of precipitation in early summer.

The main finding is that once initialized with late-spring conditions and despite maintaining constant external forcing on the system (e.g., insolation and SSTs), the simulated precipitation and circulation are able to evolve driven only by internal land-atmosphere processes and the mediation of soil hydrology. A large-scale equilibrium state is reached after approximately 270 days, and it is characterized by precipitation and circulation closely resembling mid-summer climatological conditions, when the monsoon is in full swing. As a result, intense and widespread monsoon rains over central and northern India are able to develop in the May-like state instead of June (or even later) as in the control run with seasonally-varying forcing. In other words, May boundary conditions would potentially allow monsoon rainfall to migrate northwestward if sustained for a sufficiently long period to let slow surface hydrological processes to fully exert their impact. Notice, however, that insolation also increases significantly from May to June in the seasonal run, contributing to the difference in the time scales (i.e., the time to establish a June-like regime) between the perpetual and the seasonal runs.

The northwestward inland propagation of the precipitation front comprises a succession of 35-50 day coupled oscillations between soil moisture, precipitation, and circulation. The oscillatory regime is self-sustained and entirely due to the internal dynamics of the system.

Additionally, these results indicate that the land-atmosphere system in May is far from being in equilibrium with the external forcing. The associated northwestward migration of the rain band, lagging behind insolation by the effect of slow surface hydrological processes, is pivotal for the existence of dry arid regions to the west (e.g., Xie and Saiki 1999). In turn, the intense heating over the semi-arid areas of Pakistan and northwestern India contributes to determining a strong longitudinal heating gradient which is a key factor for the overall progression of the monsoon front.

In contrast to the May perpetual experiment, minor changes in the precipitation regime are found when the model is initialized in early spring or mid-summer: in March insolation and SST are not large enough to allow convection to move northward, whereas in July precipitation a substantial westward migration of precipitation is restrained by the pattern of surface heating.

These findings, based on a state-of-the-art atmospheric model as well as its realistic configuration (i.e., land-sea distribution, orography, etc.) and advanced physical parameterizations (i.e., a multi-layer soil model), represent an important step for a more comprehensive understanding of the impact of land-atmosphere interactions on the actual monsoon evolution. At the same time, building on previous studies, we expect the physically and dynamically consistent picture described here to be robust across different models, although minor quantitative differences might arise due to specific parameterizations.

We acknowledge that the linear decomposition of the annual cycle into (external and internal) individual forcing factors is clearly a first-order approximation to the real climate system, in that, for example, neglects the existence of nonlinearities in the coupled system and by specifying SSTs it does not allow two-way air-sea interactions (e.g., Kirtman and Vecchi 2011). Nevertheless, this separation into fundamental building blocks is crucial for improving our understanding of basic physical processes and their significance in the more complex monsoon system, as well as their representation in models. Additionally, these findings have a bearing on the understanding of the monsoon variability over a range of time scales. At the intraseasonal scale, the expectation rests on the fact that the seasonal mean

precipitation over the continent depends strongly on the duration of the 30-60-day dry-wet phases of the monsoon (e.g., Annamalai and Slingo 2001). The striking similarity of the difference of precipitation between active and break phases and Figs. 3c and 6 is suggestive of an important forcing of the land and of regional hydrological processes. In terms of interannual variability, the latter has long been interpreted as a modulation of the annual cycle and is strongly affected by the annual cycle of the basic state (e.g., Suhas et al. 2012). A large fraction of the monsoon interannual variability is attributable to internal dynamics associated with soil moisture positive feedbacks (e.g., Meehl 1994; Goswami 1998). This has also potentially large benefits for improving regional precipitation forecasts (e.g., Koster et al. 2004).

Finally, important implications follow from a climate change perspective. The unsteady nature of the onset phase of the monsoon and the dependency of its migration on regional hydrological processes make northwestern India particularly susceptible to variability and changes. In turn, the northwestern semi-arid areas might play an increasingly important role in the future via modulation of its intense pre-monsoon surface heating by land-use change (e.g., Bollasina and Nigam 2011b) or by aerosol forcing on the regional surface energy balance.

Acknowledgements

The authors would like to thank Kirsten Findell and Ron J. Stouffer for reviewing an earlier version of the manuscript, as well as two anonymous reviewers for their insightful comments which helped to improve the manuscript. We also thank Chris Golaz for providing the data of the AM3 simulation with climatological SST.

References

Abbot DS, Emanuel KA (2007) A tropical and subtropical land-sea-atmosphere drought oscillation mechanism. J Atmos Sci 64: 4458-4466

Annamalai H, Slingo JM (2001) Active/break cycles: diagnosis of the intraseasonal variability of the Asian summer monsoon. Clim Dyn 18: 85–102

Biasutti M, Battisti DS, Sarachik ES (2003): The annual cycle over the tropical Atlantic, South America, and Africa. J Clim 16: 2491-2508

Bollasina M, Ming Y (2012) The general circulation model precipitation bias over the southwestern equatorial Indian Ocean and its implications for simulating the south Asian monsoon. Clim Dyn doi: 10.1007/s00382-012-1347-7

Bollasina M, Nigam S (2011a) The summertime "heat" low over Pakistan/northwestern India: evolution and origin. Clim Dyn 37: 957-970

Bollasina M, Nigam S (2011b) Modeling of regional hydroclimate change over the Indian subcontinent: impact of the expanding Thar desert. J Clim 24: 3089–3106

Donner LJ, et al. (2011) The dynamical core, physical parameterizations, and basic simulation characteristics of the atmospheric component AM3 of the GFDL Global Coupled Model CM3. J Clim 24: 3484–3519

Ferranti L, Slingo JM, Palmer TN, Hoskins BJ (1999) The effect of land-surface feedbacks on the monsoon circulation. QJR Meteorol Soc 125: 1527–1550

Futami M, Ohba M, Ueda H (2009): Role of soil Moisture in the seasonal progress of the Asian summer monsoon. Tsukuba Geoenvironmental Sciences 5: 3-9

Goswami BN (2005) South Asian summer monsoon: an overview. The Global Monsoon System:

Research and Forecast, C.-P. Chang, B. Wang, and N.-C. G. Lau (Eds.), WMO/TD No. 1266 (TMRP Report No. 70), 47−71

Goswami BN (1998) Interannual variation of Indian summer monsoon in a GCM: External conditions versus internal feedbacks. J Clim 11: 501-522

Goswami BN, Wu G, Yasunari T (2006) The annual cycle, intraseasonal oscillations, and roadblock to seasonal predictability of the Asian summer monsoon. J Clim 19: 5078–5099

Hagos SM, Cook KH (2005) Influence of surface processes over Africa on the Atlantic marine ITCZ and South American precipitation. J Clim 18: 4993–5010

Jiang X., Li J (2011) Influence of the annual cycle of sea surface temperature on the monsoon onset. J Geophys Res 116: D10105, doi:10.1029/2010JD015236

Kang IS., et al (2002) Intercomparison of the climatological variations of Asian summer monsoon precipitation simulated by 10 GCMs. Clim Dyn 19: 383-395

Kirtman B, Vecchi GA (2011) Why climate modelers should worry about atmospheric and oceanic weather. In: The Global Monsoon System: Research and Forecast, 2nd Edition. Chang, C.-P., Y. Ding, N.-C. Lau, R. H. Johnson, B. Wang, and T. Yasunari, Eds., World Scientific Series on Asia-Pacific Weather and Climate, Vol. 5, World Scientific Publication Company, 608 pp, pages 511-524

Koster RD, et al. (2004) Regions of strong coupling between soil moisture and precipitation. Science 305: 1138-1140

Kripalani RH, Oh JH, Kulkarni A, Sabade SS, Chaudhari HS (2007) South Asian summer monsoon precipitation variability: coupled climate simulations and projections under IPCC AR4. Theor Appl Clim 90: 133-159.

Lau, NC, Nath MJ (2012) A model study of the air–sea interaction associated with the climatological aspects and interannual variability of the south Asian summer monsoon development. J Clim 25: 839-857

Lestari RK, Iwasaki T (2006) GCM study on the roles of the seasonal marches of the SST and land-sea thermal contrast in the onset of the Asian summer monsoon. J Meteor Soc Japan 84: 69–83

Mapes BE, Liu P, Buenning N (2005) Indian monsoon onset and the Americas midsummer drought: out-of-equilibrium responses to smooth seasonal forcing. J Clim 18: 1109–1115

Meehl GA (1994) Influence of the land surface in the Asian summer monsoon: External conditions versus internal feedbacks. J Clim 7: 1033-1049

Meehl GA, Arblaster JM, Lawrence DM, Seth A, Schneider EK, Kirtman BP, Min D (2006) Monsoon regimes in the CCSM3. J Clim 19: 2482–2495

Rayner NA, Parker DE, Horton EB, Folland CK, Alexander LV, Rowell DP, Kent EC, Kaplan A (2003) Global analyses of sea surface temperature, sea ice, and night marine air temperature since the late nineteenth century. J Geophys Res 108: 4407 10.1029/2002JD002670

Saha SK, Halder S, Krishna Kumar K, Goswami BN (2011) Pre-onset land surface processes and 'internal' interannual variabilities of the Indian summer monsoon. Clim Dyn 36: 2011-2089

Shukla J, Fennessy MJ (1994) Simulation and predictability of monsoons. Proc MONEG Int Conf on Monsoon Variability and Prediction Trieste, Italy, WMO/TD-No. 619, 567–575

Srinivasan J, Gadgil S, Webster PJ (1993) Meridional propagation of large-scale monsoon convective zones. Meteor Atmos Phys 52: 15-35

Sud YC, Walker GK, Mehta VM, Lau WKM (2002) Relative importance of the annual cycles of sea surface temperature and solar irradiance for tropical circulation and precipitation: a climate model simulation study. Earth Interact 6: 1–32

Suhas E, Neena JM, Goswami BN (2012) Interannual variability of Indian summer monsoon arising from interactions between seasonal mean and intraseasonal oscillations. J Atmos Sci doi: 10.1175/JAS-D-11-0211.1

Ueda H (2005) Air-sea coupled process involved in stepwise seasonal evolution of the Asian summer

monsoon. Geog Rev of Japan 86: 825-841

Ueda H, Ohba M, Xie SP (2009) Important factors for the development of the Asian-Northwest Pacific summer monsoon. J Clim 22: 649–669

Uppala SM, et al (2005) The ERA40 reanalysis. Q J R Met Soc131: 2961-3012

Wang B, Lin Ho (2002) Rainy season of the Asian–Pacific summer monsoon J Clim 15: 386–398

Wang B, Clemens S, Liu P (2003) Contrasting the Indian and East Asian monsoons: Implications on geologic time scale. Mar Geol 201: 5–21

Webster PJ (1983) Mechanisms of monsoon transition: surface hydrology effects. J Atmos Sci 40: 2110-2124

Webster PJ, Magaña VO, Palmer TN, Shukla J, Tomas RA, Yanai M, Yasunari T (1998) Monsoons: processes, predictability, and the prospects for prediction. J Geophys Res 103: 14451-14510

Wu R, Wang B (2001) Multi-stage onset of summer monsoon over the western North Pacific. Clim Dyn 17: 277-289

Xie P, Arkin PA (1997) Global precipitation: A 17-year monthly analysis based on gauge observations, satellite estimates, and numerical model outputs. Bull Amer Meteor Soc 78: 2539-2558

Xie S-P, Saiki N (1999) Abrupt onset and slow seasonal evolution of summer monsoon in an idealized GCM simulation. J Meteor Soc Japan 77: 949–968

Xie SP, Xu H, Saji NH, Wang Y, Liu WT (2006) Role of narrow mountains in large-scale organization of Asian monsoon convection. J Clim 19: 3420–3429

Yang S, Lau KM (2006) Interannual variability of the Asian monsoon. In: Asian Monsoon, Ed. B. Wang, Springler-Praxis, 259-293

Yasunari T (2007) Role of land-atmosphere interaction on Asian monsoon climate. J Met Soc Japan 85B: 55-75

Zwiers FW, Boer GJ (1987) A comparison of climates simulated by a general circulation model when

run in the annual cycle and perpetual modes. Mon Wea Rev 115: 2626–2644

Figure captions

Figure 1: Pentad observed climatological (1981-2000 average) latitude-time variations of precipitation (mm day^{-1}, shades, average over 70°-90°E), SST (°C, black contours, average over 50°-75°E), and 850-hPa winds (m s^{-1}, average over 50°-65°E, displayed for speed above 5 m s^{-1}).

Figure 2: Time-latitude variation of precipitation (mm day^{-1}) averaged over 70°-90°E for (a) observations and (b) simulated by CTL, with the black line representing the 5 mm day^{-1} contour for each simulated year. May-average precipitation (mm day^{-1}) and 850-hPa winds (m s^{-1}) in (c) observations and (d) simulated by CTL. (e): June-May change in precipitation (mm $day^{-1,}$ with the zero contour line in grey) and 850-hPa winds (m s^{-1}) simulated by CTL. (f): average of precipitation (mm day^{-1}) and 850-hPa winds (m s^{-1}) over the first 30 days of the perpetual May experiment.

Figure 3: (a): Time-latitude cross-sections of 30-day average precipitation (mm day^{-1}, 70°-90°E average, contours every 2 mm day^{-1}, shaded above 8 mm day^{-1}), and 850-hPa winds (m s^{-1}, 50°-65°E average, displayed for speed above 5 m s^{-1}) in the May experiment. (b): Change in precipitation (mm day^{-1}, zero contour in grey) and 850-hPa winds (m s^{-1}, displayed for speed above 2 m s^{-1}) between the first two months in the May experiment. (c): As (b), but for the change between the equilibrium and the initial state. (d)-(f): As (a)-(c) but for the March experiment. (g)-(i): As (a)-(c) but for the July experiment. The black dots mark the grid points at 95% or higher significance level.

Figure 4: Time-longitude cross-sections (20°-28°N average, land-only points) of 30-day averages from the May experiment. (a): Precipitation (mm day^{-1}, shades) and 0-4 cm total liquid soil moisture content

(volumetric fraction, contours). (b): (1000-300)-hPa integrated moisture flux (kg m^{-1} s^{-1}, arrows, displayed for magnitude above 50 kg m^{-1} s^{-1}), its convergence (mm day^{-1}, shades, zero line in grey), and evaporation (mm day^{-1}, contours). (c): 900-hPa specific humidity (g kg^{-1}, shades) and surface skin temperature (°C, contours). (d): 925-hPa moist static energy (°C after dividing by c_p, the specific heat capacity at constant pressure, shades) and sensible heat flux (mm day^{-1} after multiplying by 86400 L_v^{-1} with L_v the latent heat of evaporation, contours). The black dots mark the grid points at 95% or higher significance level.

Figure 5: Pentad variations of precipitation (mm day^{-1}, blue), surface skin temperature (°C, red), sensible heat flux (W m^{-2}, purple), evaporation (mm day^{-1}, light blue), and meridional wind (m s^{-1}, black) in the May experiment. The time series are averaged over (72°-85°E, 20°-25°N; land-only points), except for the meridional wind (85°-90°E, 15°-20°N). For some variables, the original (X_O) value has been scaled to fit the same vertical axis (X_N): evaporation $E_N = 3 \times E_O$, surface temperature $T_N = 2 \times (T_O - 25)$, sensible heat flux $S_N = S_O / 7$. The long-dashed vertical yellow lines correspond to the peaks in precipitation. The short-dashed lines are the logarithmic fits to the respective time series.

Figure 6: Lead/lag regressions of pentad precipitation (mm day^{-1}, shades), surface skin temperature (°C, black contours), and 850-hPa winds (vectors, displayed for speed above 0.3 m s^{-1}) for the May experiment. Regressions are calculated with respect to a reference time series of precipitation over (72°-85°E, 20°-25°N), and are displayed at 5-day intervals from -20 days to +15 days. The lag = 0 days represents simultaneous regressions with the reference time series.

Figures

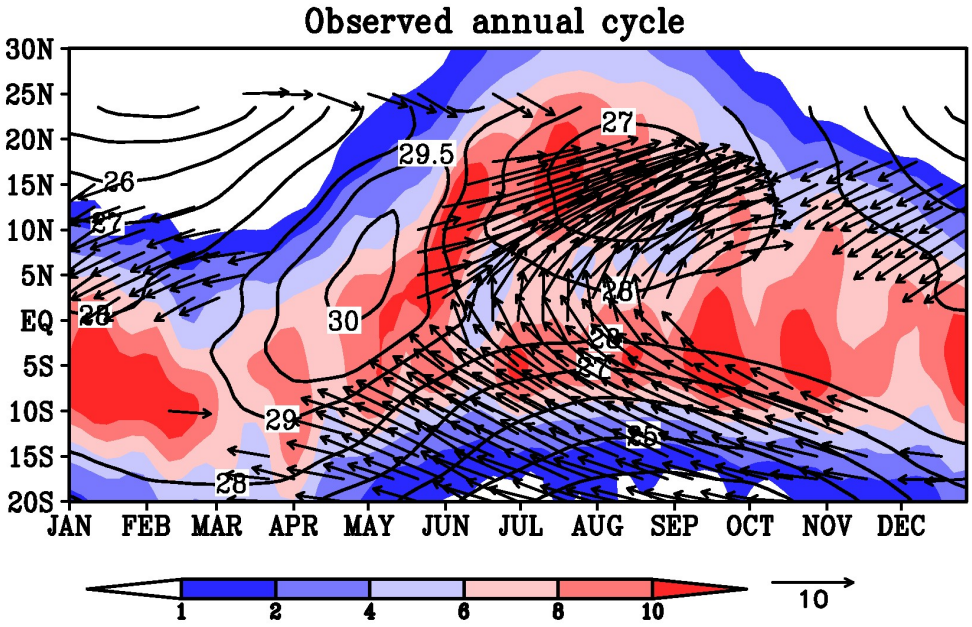

Figure 1: Pentad observed climatological (1981-2000 average) latitude-time variations of precipitation (mm day^{-1}, shades, average over 70°-90°E), SST (°C, black contours, average over 50°-75°E), and 850-hPa winds (m s^{-1}, average over 50°-65°E, displayed for speed above 5 m s^{-1}).

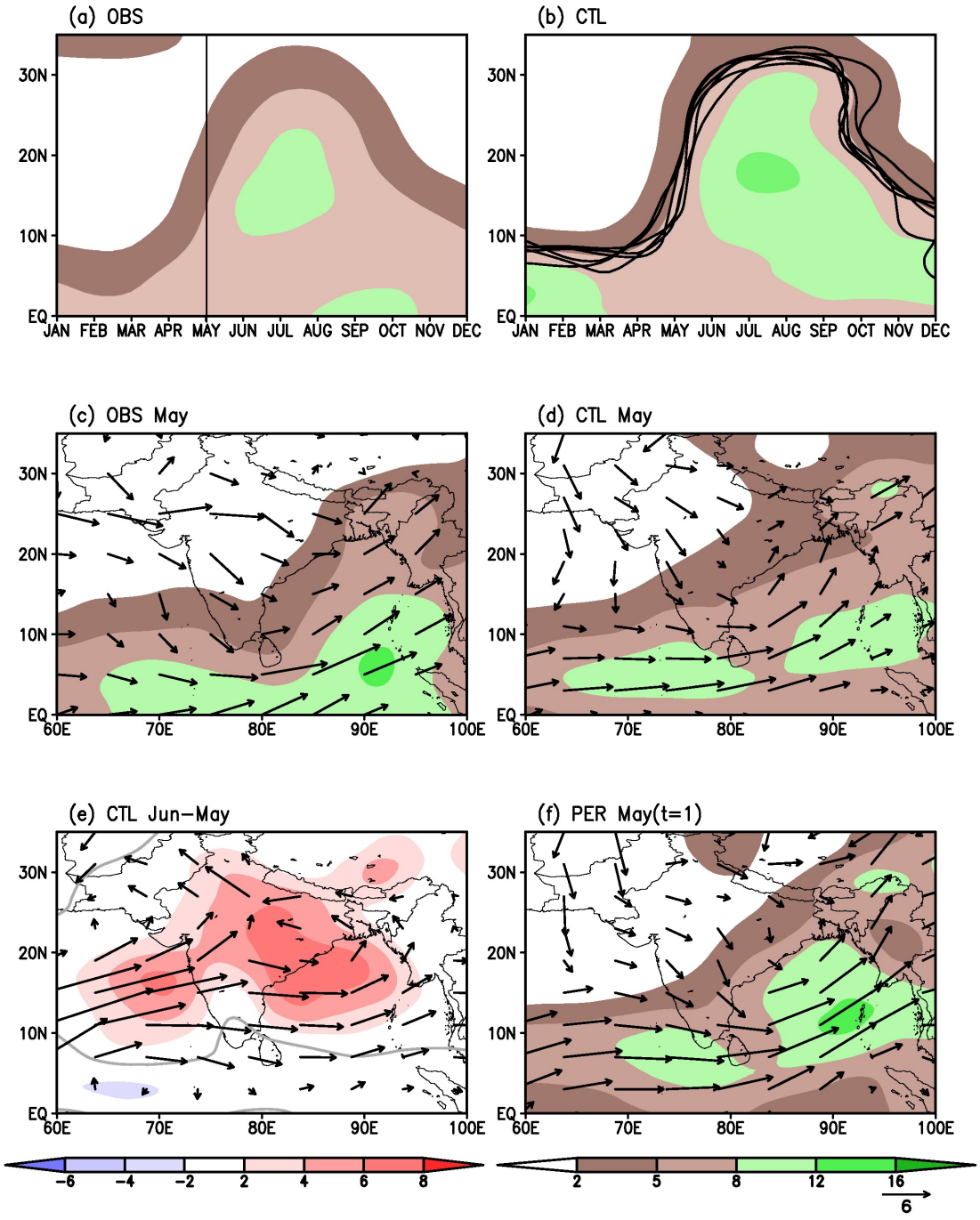

Figure 2: Time-latitude variation of precipitation (mm day^{-1}) averaged over 70°-90°E for (a) observations and (b) simulated by CTL, with the black line representing the 5 mm day^{-1} contour for each simulated year. May-average precipitation (mm day^{-1}) and 850-hPa winds (m s^{-1}) in (c) observations and (d) simulated by CTL. (e): June-May change in precipitation (mm day^{-1}, with the zero contour line in grey) and 850-hPa winds (m s^{-1}) simulated by CTL. (f): average of precipitation (mm day^{-1}) and 850-hPa winds (m s^{-1}) over the first 30 days of the perpetual May experiment.

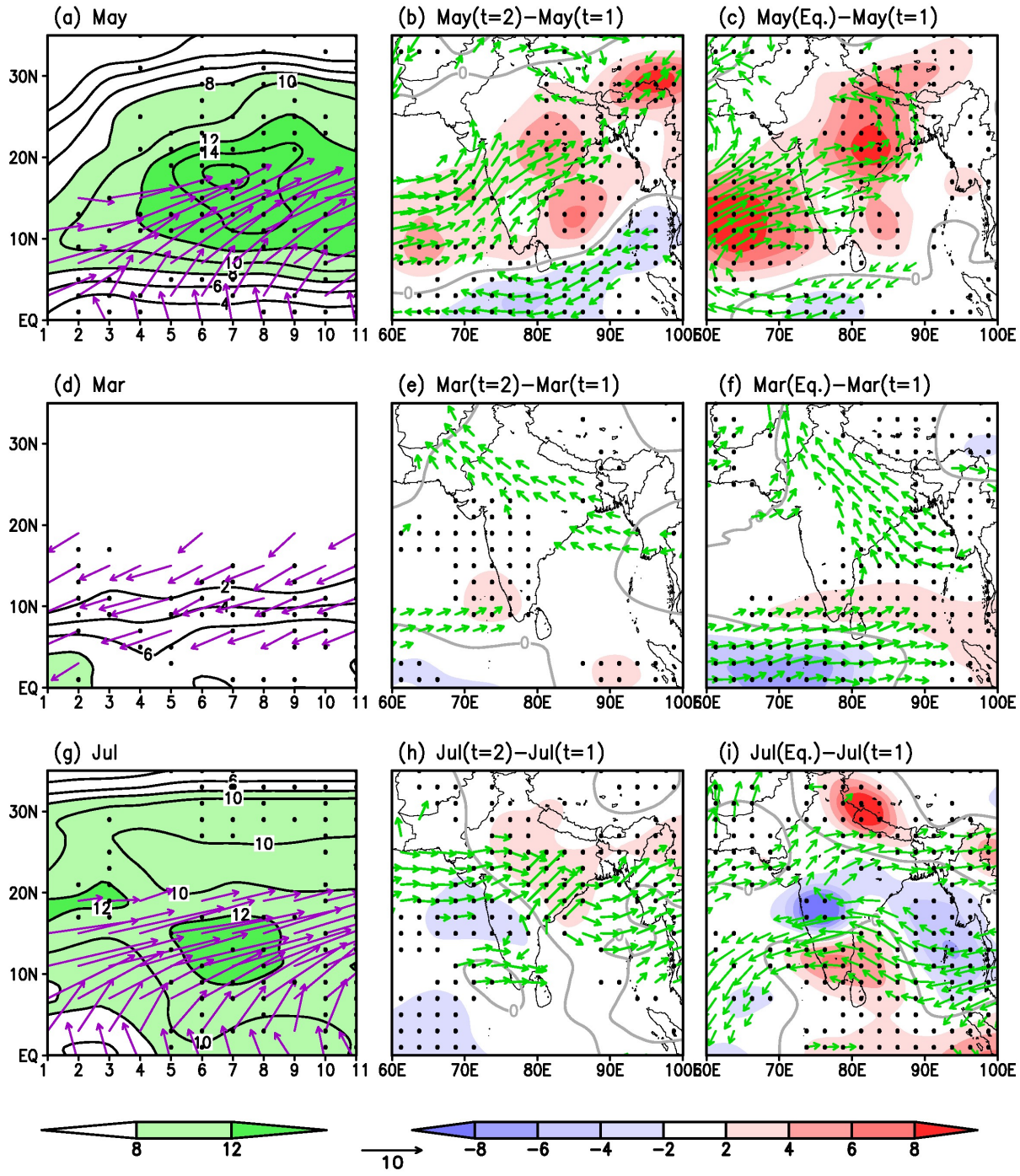

Figure 3: (a): Time-latitude cross-sections of 30-day average precipitation (mm day^{-1}, 70°-90°E average, contours every 2 mm day^{-1}, shaded above 8 mm day^{-1}), and 850-hPa winds (m s^{-1}, 50°-65°E average, displayed for speed above 5 m s^{-1}) in the May experiment. (b): Change in precipitation (mm day^{-1}, zero contour in grey) and 850-hPa winds (m s^{-1}, displayed for speed above 2 m s^{-1}) between the first two months in the May experiment. (c): As (b), but for the change between the equilibrium and the initial state. (d)-(f): As (a)-(c) but for the March experiment. (g)-(i): As (a)-(c) but for the July experiment. The black dots mark the grid points at 95% or higher significance level.

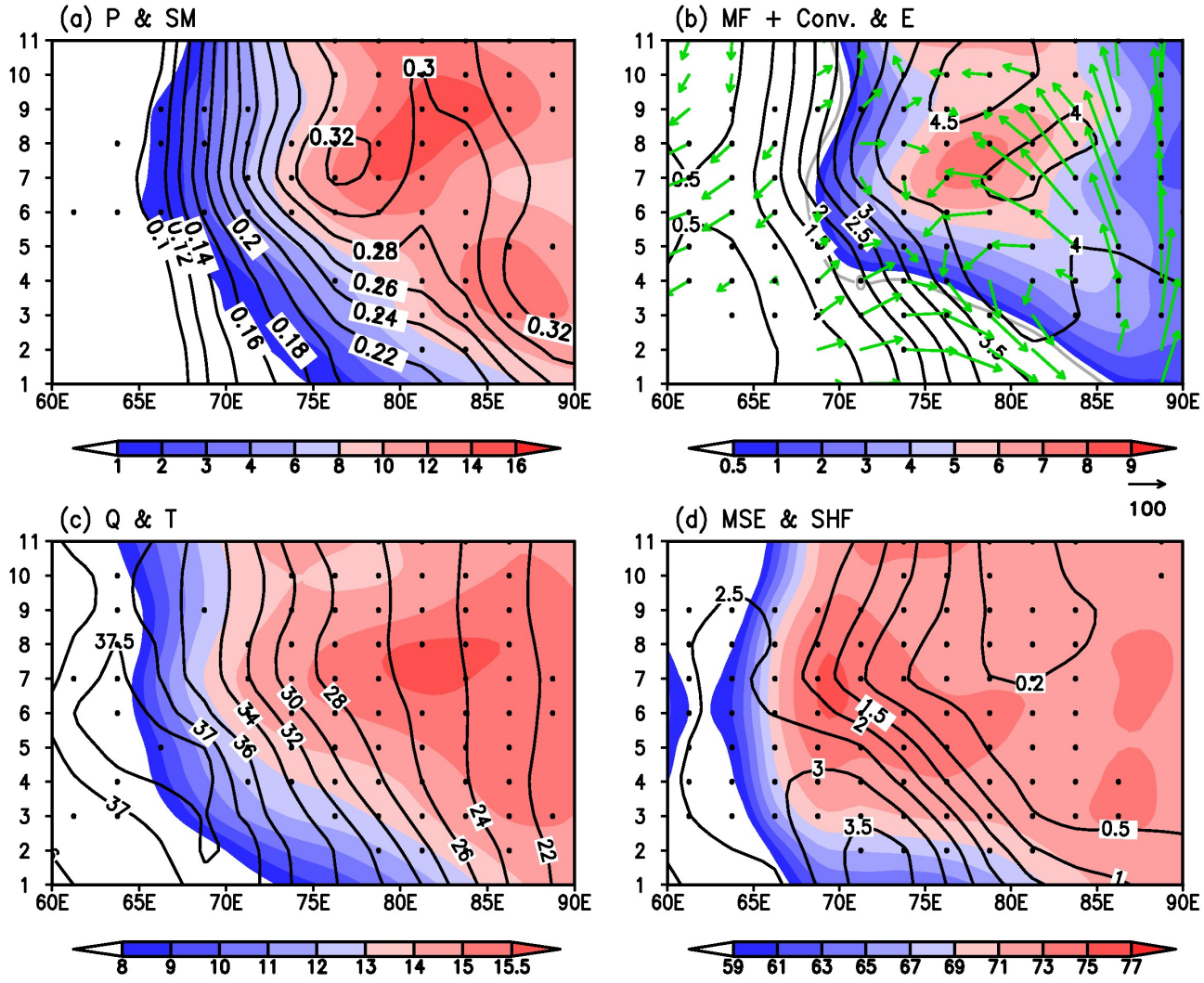

Figure 4: Time-longitude cross-sections (20°-28°N average, land-only points) of 30-day averages from the May experiment. (a): Precipitation (mm day^{-1}, shades) and 0-4 cm total liquid soil moisture content (volumetric fraction, contours). (b): (1000-300)-hPa integrated moisture flux (kg m^{-1} s^{-1}, arrows, displayed for magnitude above 50 kg m^{-1} s^{-1}), its convergence (mm day^{-1}, shades, zero line in grey), and evaporation (mm day^{-1}, contours). (c): 900-hPa specific humidity (g kg^{-1}, shades) and surface skin temperature (°C, contours). (d): 925-hPa moist static energy (°C after dividing by c_p, the specific heat capacity at constant pressure, shades) and sensible heat flux (mm day^{-1} after multiplying by 86400 L_v^{-1} with L_v the latent heat of evaporation, contours). The black dots mark the grid points at 95% or higher significance level.

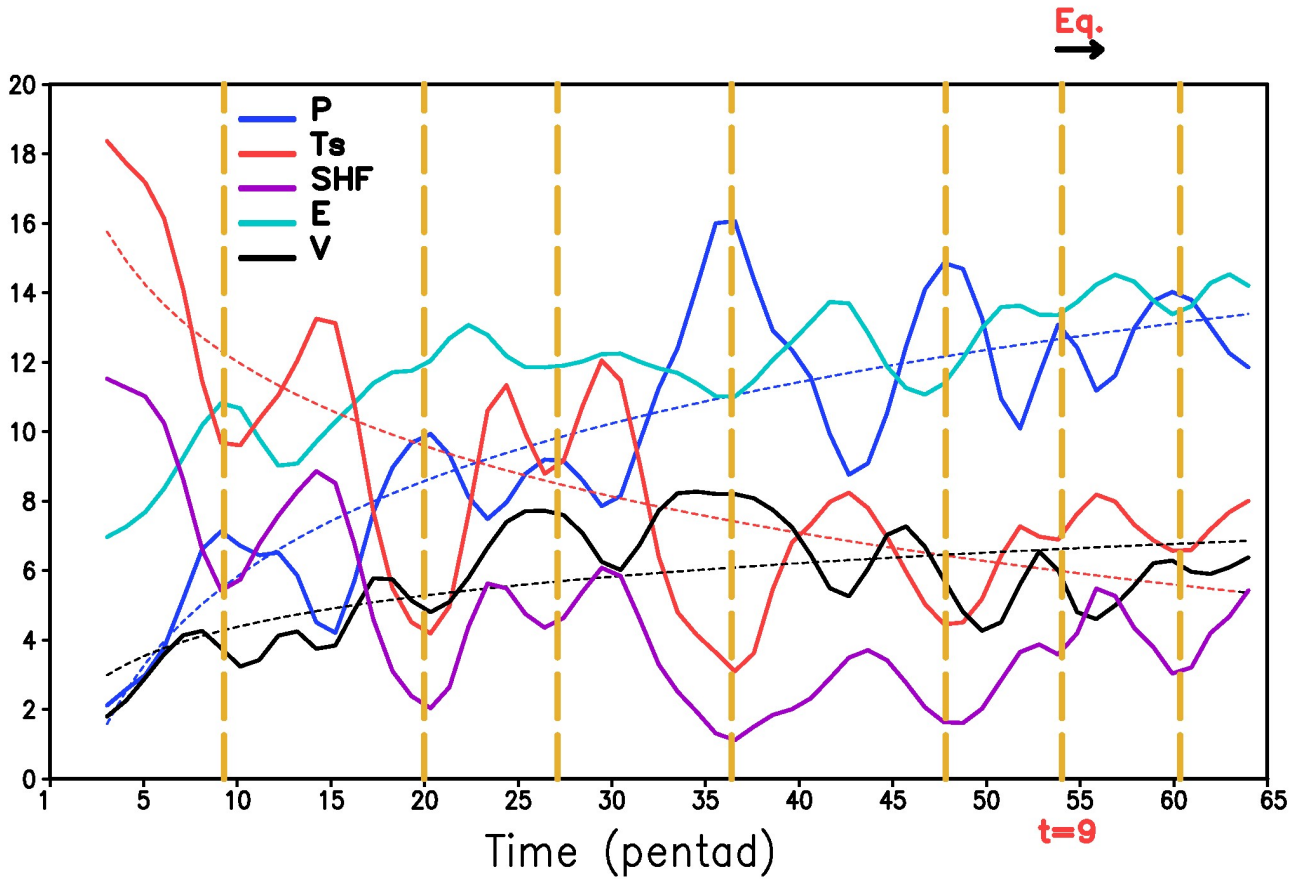

Figure 5: Pentad variations of precipitation (mm day^{-1}, blue), surface skin temperature (°C, red), sensible heat flux (W m^{-2}, purple), evaporation (mm day^{-1}, light blue), and meridional wind (m s^{-1}, black) in the May experiment. The time series are averaged over (72°-85°E, 20°-25°N; land-only points), except for the meridional wind (85°-90°E, 15°-20°N). For some variables, the original (X_O) value has been scaled to fit the same vertical axis (X_N): evaporation $E_N = 3 \times E_O$, surface temperature $T_N = 2 \times (T_O - 25)$, sensible heat flux $S_N = S_O / 7$. The long-dashed vertical yellow lines correspond to the peaks in precipitation. The short-dashed lines are the logarithmic fits to the respective time series.

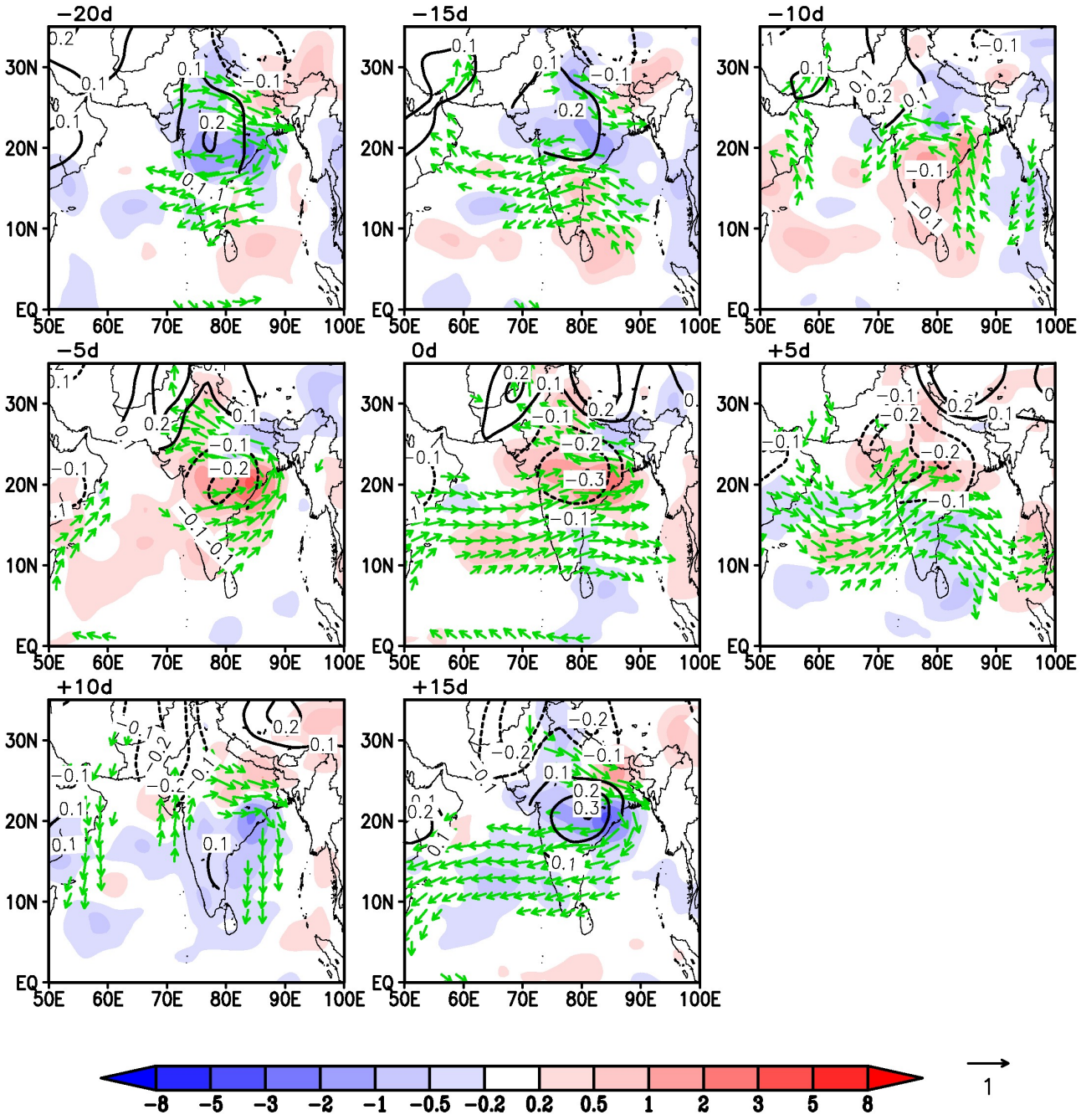

Figure 6: Lead/lag regressions of pentad precipitation (mm day^{-1}, shades), surface skin temperature (°C, black contours), and 850-hPa winds (vectors, displayed for speed above 0.3 m s^{-1}) for the May experiment. Regressions are calculated with respect to a reference time series of precipitation over (72°-85°E, 20°-25°N), and are displayed at 5-day intervals from -20 days to +15 days. The lag = 0 days represents simultaneous regressions with the reference time series.